Available online at www.sciencedirect.com

SciVerse ScienceDirect

Ceramics International 39 (2013) 7709–7716

CERAMICS INTERNATIONAL

www.elsevier.com/locate/ceramint

Preparation, optimization and characterization of low cost ceramics for the fabrication of dense nickel composite membranes

Amrita Agarwal, Murali Pujari, R. Uppaluri*, A. Verma

Department of Chemical Engineering, Indian Institute of Technology Guwahati, Guwahati-781039 Assam, India

Received 11 February 2013; accepted 10 March 2013
Available online 16 March 2013

Abstract

This article addressed a broad research methodology for the development of low cost ceramics to serve as functional supports for dense metal composite membranes. The experimental challenge of this study is to work with laboratory fabricated supports characterized with lower combinations of average pore size (50–70 nm) and lower effective porosity (0.012) and hence lower surface area for activation and plating reaction. Apart from fabrication parameters, the research emphasis has been towards ensuring morphological fitness of the ceramic support, good corrosion resistance and continuous enhancement in pore densification during prolonged nickel electroless plating of about 24 h. Surface and physical characterization using LPSA, BET, FTIR, XRD, FESEM and nitrogen permeation techniques yielded valuable insights. It has been observed that the sonication of the raw membrane support in alkaline conditions enormously contributed towards good corrosion resistance during nickel ELP. The morphological fitness of the ceramic support has been targeted by assuming a combination of Knudsen and Viscous diffusion through the membrane support and activated diffusion through the dense nickel film. Thereby the morphological fitness is ensured by evaluating whether or not nickel film nitrogen flux values are lower than the support fluxes.

Keywords: Electroless plating; Surfactant; Average flux; Nickel membrane

1. Introduction

Amongst organic and inorganic/metal membranes, the latter are highly promising towards various industrial schemes that involve higher processing temperatures and corrosive environments. Inorganic/metal membranes have been further classified into porous and dense composite membranes. Typically, alumina, carbon or stainless steel are commonly used materials for metal composite membranes [1–4]. Amongst these, sintered stainless steel membranes have received attention due to possessing higher durability as a filter medium for superior separations and consistent performance under extreme process conditions and high operating temperatures. However, large scale applications of stainless steel membranes are highly expensive when compared to ceramic membranes and fabrication research is also equally focused towards utilizing ceramic membrane supports [5].

Presently, metal ceramic composite membranes have been suggested for several applications including TiO_2 recovery from waste water streams [6], production of ultrapure gases for special applications [7], bacteriostatic treatment [8], asymmetric supports for dense palladium (Pd) composite membranes [9] and hydrogen separation [10]. Presently companies such as Mykron, Entegris and Mott Corporation fabricate ceramic composite membranes for several commercial applications. Typically, amongst ceramics, alpha-alumina supports are used for Pd membrane fabrication. However, alpha-alumina being expensive, its large scale application for Pd composite membranes is also bound to contribute higher costs for the composite membrane and hence there is a need for research into low cost ceramic supports for dense Pd membrane fabrication.

The consistent performance of ceramic membranes to serve as functional supports for dense Pd membranes needs to ensure their compatibility from several perspectives. First, membranes with lower pore size, good porosity and narrow pore size distribution are required so as to reduce the critical thickness of Pd required for the realization of dense membrane. Second, the membrane shall possess excellent corrosion resistance to withstand conditions during alkaline nickel electroless plating as well as industrial processing schemes. Third, the support shall enable continuous enhancement in pore densification during sequential metal deposition using electroless plating. Fourth, the

*Corresponding author. Tel.: +91 3612582260; fax: +91 3612582291.
E-mail address: ramgopalu@iitg.ernet.in (R. Uppaluri).

0272-8842/$ - see front matter © 2013 Elsevier Ltd and Techna Group S.r.l. All rights reserved.
http://dx.doi.org/10.1016/j.ceramint.2013.03.024

nickel film shall provide lower gas flux when compared to the support flux and therefore the support morphological parameters need to be fine-tuned during fabrication research. A critical review of literatures available for dense Pd membranes research indicates the lack of integrated methodologies and approaches towards research in the functional supports [1,9]. The cost of a composite membrane is a function of both metal film and the support and hence, cost reductions in support fabrication along with metal film deposition would be highly useful to drive economic competitiveness of the metal ceramic composite membranes.

Combinatorial performance characteristics of metal ceramic membranes were addressed by our research group [11,12]. However these studies were not directed towards support morphological issues for dense membrane fabrication. In addition time dependency of process and membrane parameters was also not reported. Based on our past experience with electroless plating (ELP) and its mass transfer coupled variance this work anticipates to obtain useful insights towards dense metal membrane fabrication with supports characterized with lower pore size and lower porosity.

Considering nickel as the target plating metal, a conceptual research methodology has been outlined that systematically addresses the experimental and theoretical insights for the realization of dense metal composite membranes. The laboratory fabricated porous supports were characterized with lower average pore size (50–70 nm) and lower effective porosity (0.012), so as to provide most challenging scenario for the plating processes towards maximum pore densification. Using the concept of lower gas transport resistance of the metal film with respect to the support, the next section elaborates upon the justification to select the support pore morphology (50–70 nm) for targeting dense metal composite membranes.

2. Morphological fitness of the ceramic support

Using nickel as the electroless plated metal, the ultimate objective of the research was to provide insights in plating rate enhancement methods for contributing towards research in dense nickel composite membranes. This was also due to the fact that flux data for dense nickel membranes was not available in the literature. An important functional prerequisite for metal composite membrane was that the metal (Ni) film flux (H_2) shall always be lower than the porous support flux. Since nickel flux increased with temperature, maximum nickel flux was achieved at the highest possible operation temperature and minimal metal thickness. For the present case, these values were assumed to be 550 °C and 1 μm, respectively. The model based maximum hydrogen flux achievable through the dense Ni film was evaluated using the expression:

$$J_{H_2}^{\mathrm{mod}} = \frac{Perm_{\mathrm{lit}}}{\delta_{ass}} \times \delta_{\mathrm{lit}} \times A_m \times (P_{\mathrm{ret}}^{n'} - P_{\mathrm{per}}^{n'}) \tag{1}$$

where $Perm_{\mathrm{lit}}$ and δ_{lit} correspond to the theoretical dense Ni film permeability and thickness in the composite membrane. The dense nickel film permeability was estimated using the expression [13]:

$$Perm_{\mathrm{lit}} = 3.35 \times 10^{-7} \exp\left(\frac{-54.25 \times 10^3}{RT}\right) \tag{2}$$

Assuming a combination of Knudsen and viscous diffusion, for a given membrane morphological parametric combination of d_p and (ε/q^2), the average hydrogen flux through the porous support was evaluated using the expression:

$$J_{H_2}^{\mathrm{sup}} = \left(\frac{2.133}{2}\frac{d_p v}{l}\left(\frac{\varepsilon}{q^2}\right) + \frac{1.6}{4}\frac{d_p^2}{pl\eta}\left(\frac{\varepsilon}{q^2}\right)\overline{P}\right)\frac{\Delta P}{P_2} \tag{3}$$

Assuming that the metal ceramic composite membrane was feasible only when the metal film flux was at least 10% lower than that of the support hydrogen flux, an inequality constraint needs to be satisfied, which was expressed as:

$$\frac{(J_{H_2}^{\mathrm{sup}} - J_{H_2}^{\mathrm{mod}})}{J_{H_2}^{\mathrm{sup}}} \times 100 \geq 10 \cdots \forall \Delta P \tag{4}$$

To validate the above system of equations in a systematic format, a simple procedure was followed to evaluate the feasibility of the support morphology:

(i) Using Eq. (1), determine $J_{H_2}^{\mathrm{mod}}$ vs. ΔP data for assumed membrane parameters from the literature.

(ii) Using Nitrogen gas as the transport gas, conduct single gas permeation experiments and obtain $J_{N_2}^{\mathrm{sup}}$ (experiment) vs. ΔP. Using the experimental data and Eq. (3), determine membrane morphological parameters experimentally (d_p^{sup} and (ε/q^2))

(iii) For a specified value of d_p^{sup} or (ε/q^2), determine the minimum value of (ε/q^2) min or d_p^{min} to satisfy the following optimization problem defined in terms of dense Ni film and support hydrogen flux:

$$\begin{aligned}
&\mathrm{Min} = \sum_{i=1}^{\Delta P\max} \\
&E_i = \frac{(J_{\mathrm{Ni}_{H_2}} - J_{\mathrm{sup}_{H_2}})}{J_{\mathrm{Ni}_{H_2}}} \times 100 \\
&J_{H_2}^{\mathrm{mod}} = \frac{Perm_{\mathrm{lit}}}{\delta_{ass}} \times \delta_{lit} \times A_m \times (P_{\mathrm{ret}}^{n'} - P_{\mathrm{per}}^{n'}) \\
&J_{H_2}^{\mathrm{sup}} = \left(\frac{2.133}{2}\frac{d_p v}{l}\left(\frac{\varepsilon}{q^2}\right) + \frac{1.6}{4}\frac{d_p^2}{l\eta}\left(\frac{\varepsilon}{q^2}\right)\overline{P}\right)\frac{\Delta P}{P_2} \\
&E_i \geq 10 \ \forall \ i \\
&0 \leq \left(\frac{\varepsilon}{q^2}\right)_{\mathrm{sup}}^{th} \leq 1 \ (OR) \ d_p^{\mathrm{min}} \geq 0
\end{aligned} \tag{5}$$

(iv) The support morphological parameters were regarded to be feasible for plating after either one of the following two constraints were satisfied:

$$d_p^{\mathrm{sup}} \geq d_p^{\mathrm{min}} \ \mathrm{OR} \ \left(\frac{\varepsilon}{q^2}\right)^{\mathrm{sup}} \geq \left(\frac{\varepsilon}{q^2}\right)^{\mathrm{min}} \tag{6}$$

Based on our research a case study was presented below to illustrate the above procedure. For an assumed Ni film thickness

of 5 μm, and an evaluated dense Ni film permeability of 1.207×10^{-10} (mol/m/m^2/s/Pa$^{0.5}$) [13], the theoretical Ni dense film hydrogen flow rate varied from 4.81×10^{-4}–2.02×10^{-2} (lit/min) for a trans-membrane pressure difference of 0.1–10 atm. The room temperature N_2 permeation data for the support varied from 4.81×10^{-4}–2.02×10^{-2} (lit/min) for a trans-membrane pressure difference variation from 0.1 to 10 atm. Calculations using the N_2 gas permeation data at room temperature indicated that the membrane morphological parametric values were $d_p^{sup} = 57$ nm and $(\varepsilon/q^2)^{sup} = 0.012$. Assuming d_p^{exp} as d_p^{mod}, the solution of the optimization model (Eq. (4)) inferred that (ε/q^2) min = 0.003063, which was lower than the value obtained from experimental data i.e., $(\varepsilon/q^2)^{sup} = 0.012$. Thus, the support morphology was concluded to be feasible for proceeding towards electroless plating research. Additional trade-offs associated to dense film thickness variations are presented in the results and discussion section of this article. The next section elaborates upon the experimental investigations towards support fabrication and ELP for dense membrane fabrication.

3. Experimental

3.1. Low cost ceramic membranes

Laboratory made disk shaped ceramic substrates with a diameter of 36 mm and thickness of 3.5 mm were prepared for all experiments. The supports were fabricated at a pressure of 4.9 MPa using a hydraulic press (Make—Velan Engineering) by the dry compaction method. The support possessed a pore size d_p^{sup} and effective porosity (ε/q^2) of about 50–70 nm and 0.012 nm, respectively.

Seven inorganic raw materials viz. kaolin, feldspar, quartz, sodium carbonate, pyrophyllite, boric acid and sodium metasilicate were used in the fabrication of ceramic membrane supports. Kaolin was obtained from CDH Ltd., India, feldspar and pyrophyllite from National Chemicals, India, quartz from Research-lab Fine Chem Industries, India, sodium metasilicate from SD Fine-chem Ltd., India and the other inorganic precursors (sodium carbonate and boric acid) were obtained from Merck Ltd., India. Composition of various raw materials along with their average particle size (as shown in Fig. 1) were mentioned in Table 1. The fabrication methodology consists of the following hierarchical steps: mixing of raw materials to make a paste; casting of the paste into circular moulds; drying of the raw discs; sintering; polishing of the membranes and ultrasonically cleaning. All membranes were prepared by sintering at 900 °C with a controlled heating/cooling rate (1.5 °C/min).

3.2. Surface and flux characterization

Raw material, support and membrane characterizations were carried out by laser particle size analyzer (LPSA), Brunauer Emmett Teller (BET) surface area analyzer, fourier transform infrared spectroscopy (FTIR), X-ray diffraction (XRD) and field emission scanning electron microscopy (FESEM).The mean pore size of the bulk membrane was estimated from

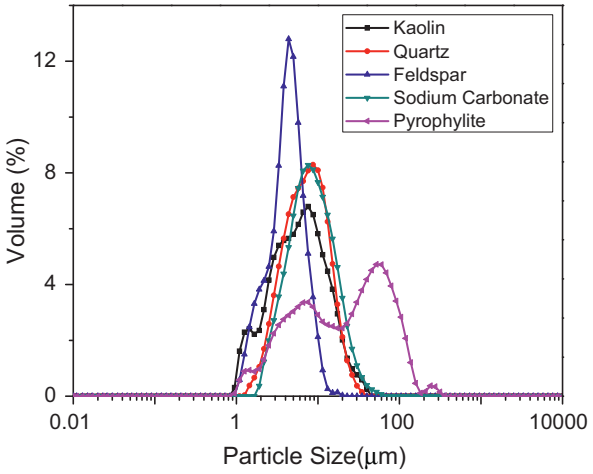

Fig. 1. Particle size distribution for different raw materials.

Table 1
Composition of raw materials for the fabrication of ceramic membrane supports.

Material	Composition on dry basis (wt %)	Average particle size (μm)
Kaolin	40	5.50
Feldspar	15	3.46
Quartz	15	7.72
Na_2CO_3	10	7.59
Pyrophyllite	10	20.36
Boric acid	5	–
Sodium metasilicate	5	–

nitrogen permeation experiments. Membrane porosity was determined by weight gain method. The flux of the composite membranes was anticipated from nitrogen permeation data and the experimental setup was similar to the one as discussed by Bulasara et al. [12]. For all permeation experiments, high purity N_2 (99.99% obtained from Assam Air Products Ltd., Guwahati) was used for an effective permeation area of1.0173×10^{-3} m^2.

3.3. Electroless plating

Electroless plating technique was taken up for nickel deposition with the typical compositions summarized in Table 2. Prior to plating, seeding was carried on which involved the conventional procedure of activation and sensitization of the support with palladium seeds. Eight sequential 1 h nickel deposition steps with a nickel concentration of 0.08 (mol/L) were taken up to yield the nickel ceramic composite membranes. A 50% excess hydrazine hydrate was used as a reducing agent. The plating was carried on a water bath maintained at 80 °C and the plating characteristics were investigated at a loading ratio of 203 (cm^2/L). Four different cases as listed in Table 3 were focused for this work which involved membranes prepared with sonication assisted ELP (M_1), surfactant assisted ELP (M_2), NaOH treated support and

Table 2
Typical composition of conventional and surfactant induced nickel electroless plating baths.

S. no.	Component	Formula	Role	Amount
1.	Nickel sulfate	$NiSO_4 \cdot 7H_2O$	Source of nickel	0.08 mol/L
2.	Hydrazine Hydrate	$H_2NNH_2 \cdot H_2O$	Reducing agent	50% excess
3.	Trisodium citrate	$Na_3C_6H_5O_7 \cdot 2H_2O$	Stabilizer	0.2 mol/L
4.	Sodium Hydroxide	NaOH	pH	10–12
5	Cetyltrimethylammonium bromide	$(C_{16}H_{33})N(CH_3)_3Br$	Dispersion	1.2 g/L

surfactant assisted ELP (M_3) and NaOH treated support and sonication assisted ELP (M_4) study.

Prior to plating, membranes M_3 and M_4 were treated. The treatment involved etching of the membrane in NaOH solution of pH 12 in a sonicator bath (Elmasonic, S30 H) under degas mode of continuous operation for 6 h at 80 °C (plating temperature). This modified the support morphology and enhanced support corrosion resistance. Subsequently, the support pore size (based on nitrogen gas permeation) enhanced from 50–70 nm to 90–120 nm, respectively. However when sodium hydroxide treatment was carried without sonication and degas mode in a water bath maintained at 80 °C, the improvement in support morphology was not sufficient enough to avoid negative flux trends. For all cases, membrane supports with similar average flux values were chosen to maintain coherence amongst various performance characteristics.

3.4. Evaluation of plating characteristics

The performance assessment of various plating baths for fabricating dense nickel membranes was characterized by the determination of parameters namely average trans-membrane flux $\overline{J}$ and percent pore densification *PPD*(%).

The nitrogen flux through the membrane (J) at varying pressure was evaluated from the volumetric flow rate data

$$J = \frac{Q}{A_m}$$

where Q represents the volumetric flow rate in LPM, A_m the permeable area of the membrane in m^2 and J the flux through the membrane in (mol/m^2/s)

$$\overline{J} = \frac{\int_{P_1}^{P_2} JdP}{P_2 - P_1}$$

where $\overline{J}$ represents the average flux through the membrane, $\int_{P_1}^{P_2} JdP$ corresponds to the area under the curve of a plot between the membrane flux (mol/m^2/s) and pressure (psi).The term $P_2 - P_1$ corresponds to the trans-membrane pressure drop. Pore densification during the plating process was defined as the fractional volume of the pores covered by the deposited metal and it was expressed as a time dependent expression

$$PPD_i = \frac{\overline{J}_0 - \overline{J}_i}{\overline{J}_0} \times 100$$

where $\overline{J}_0$ represents the average flux through the support and $\overline{J}_i$ represents the average flux through the membrane after ith hour of nickel plating. *PPD* calculations were carried using the average flux data because they provide appropriate time dependency as compared to the *PPD* calculated using the pore diameter procedure in the literature [12].

Table 3
Summary of various cases investigated for the development of low cost ceramic membranes.

Case	Type of support	Type of ELP
M_1	Raw	Sonication
M_2	Raw	Surfactant
M_3	Treated	Surfactant
M_4	Treated	Sonication

4. Results and discussions

4.1. Surface characterization

The major raw materials i.e., kaolin, quartz, feldspar, sodium carbonate and pyrophylite used for the membrane fabrication process were characterized using laser particle size analyzer (Make: Malvern; Model: Mastersizer 2000, UK). Fig. 1 presents the particle size distribution of the raw materials which were the building stones for the ceramic support. It was observed that average particle size of kaolin, quartz, feldspar, sodium carbonate and pyrophylite were 5.50 μm, 7.72 μm, 3.46 μm, 7.59 μm and 20.36 μm, respectively.

The BET surface area and pore size of the support material was determined by N_2 adsorption desorption isotherm at 77 K by using a surface area analyzer (Beckman-Coulter; Model: SA3100). Prior to measurement, the samples were degassed at 200 °C in vacuum for 60 min. The adsorption/desorption isotherms of the support material was shown in Fig. 2(a). The isotherms were of type III and H_3 hysteresis loop was observed that gave rise to slit-shaped pores according to IUPAC [14]. Based on BET, the pore size distribution as a function of volume percentage of pores of the support was shown in Fig. 2(b). The average pore size as evaluated from Barrett–Joyner–Halenda (BJH) pore volume distribution was found to be 35 nm which was close to that evaluated from nitrogen permeation (50–70 nm). The BET surface area of support was 2.712 m^2/g and total pore volume was 0.0156 mL/g with no micropore volume.

The fourier transform infrared spectra recorded from wave number 4000 to 500 cm^{-1} using IR Affinity—1 spectrometer as shown in Fig. 3. Characteristic peaks of kaolin were

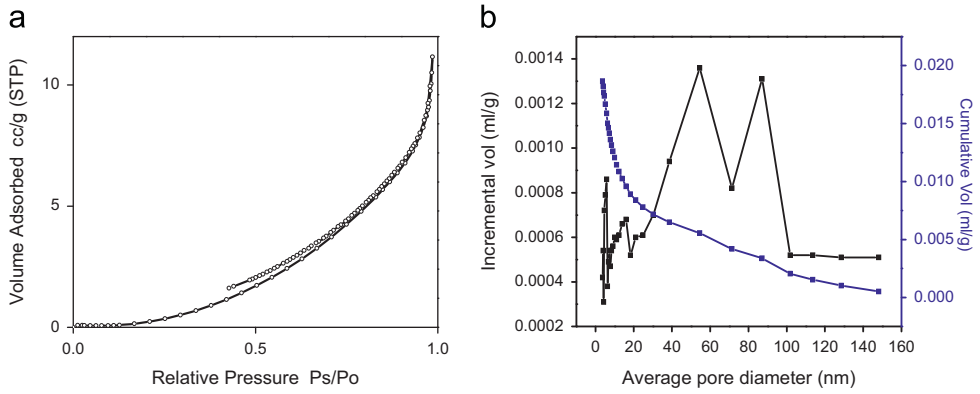

Fig. 2. (a) Nitrogen adsorption/desorption isotherms of the ceramic support material (b) Pore size distribution of the ceramic support by BET method.

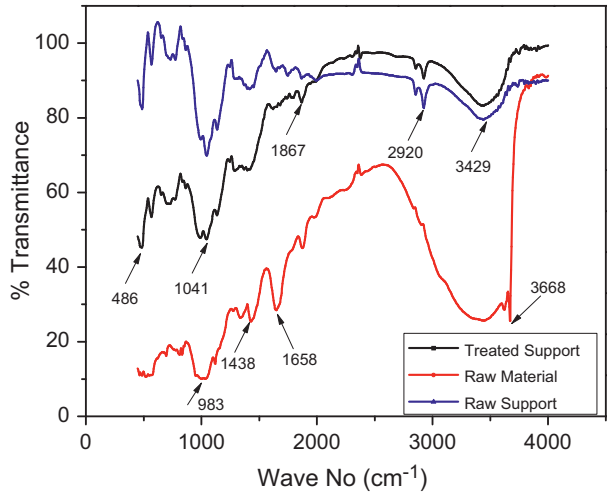

Fig. 3. FTIR Spectral analysis of various ceramic supports and raw material.

observed at 3668 cm^{-1} corresponding to the OH^- stretching vibration for the raw material. After sintering of the raw material mixture at 900 °C for 4 h, the OH^- vibration peaks at 3668 cm^{-1} decreased suggesting that the calcination of kaolin to calcined kaolin was not complete [15]. Bands at 2920 cm^{-1} were assigned to C–H bonds which were visible only after sintering and peak at 1658 cm^{-1} was attributed to C=C bonds. Further H_2O stretching was seen at 1658 cm^{-1} for the raw material which disappeared after sintering. Bands at 1041 cm^{-1} and 983 cm^{-1} were assigned to Si–O bonds. Absorption at 486 cm^{-1} was assigned to Si–O–Al [16].

The X-ray diffractograms were recorded by a Bucker X-ray D8 advance diffractometer with a Cu-K_α radiation (λ=1.54056) at 45 kV and 40 mA, respectively with scan rate of 0.5 $s \times step^{-1}$ with an increment of 0.05. The X-ray diffractograms were collected in the range of 5–75°. Phase analyses of the diffraction profiles were done using ICDD-JCPDS database and the crystallite size of the samples were calculated using Scherer's formula: $d = 0.9\lambda/\beta\cos\theta$ where d signifies the crystallite size, λ refers to the wavelength of radiation (λ=1.54056), β refers to the full width of half-maximum intensity of corrected peak and θ the peak position.

Fig. 4(a) presents the XRD patterns of raw material mixture, sintered raw support, sintered treated support and the nickel membrane. The phases for kaolin, quartz and calcium carbonate appeared in the raw material mixture. It was observed that the peak intensity of the main intense peak of quartz (2θ=26.75°) significantly increased with sintering, thereby indicating that the crystalinity of the quartz increased as compared to raw material, which was further more significant after NaOH treatment. The XRD pattern clearly indicated that NaOH treatment played a vital role in increasing the crystalinity of quartz and thereby enhancing the porosity of the membrane. Further on sintering it was observed that due to the transformation of kaolinite to metakaolinite the peak corresponding to kaolin disappeared [8].

Similarly the peak corresponding to calcium carbonate also disappeared on sintering due to thermal decomposition. The new phases that appeared in the XRD pattern were anorthite ($CaO \cdot Al_2O_3 \cdot 2SiO_2$) and mullite ($3Al_2O_3 \cdot 2SiO_2$).

Fig. 4(b) replicates the XRD pattern of Ni plating to clearly visualize the nickel peaks. The metallic nickel peaks appeared at diffraction angle 2θ=44.6° and 52° due to the diffraction of (1 1 1) and (2 0 0) plane [Pdf No 00-001-1260] along with the quartz peaks. It was observed that the peak intensity of quartz significantly decreased after nickel deposition due to plating of nickel on quartz particle thereby reducing the crystalinity of the quartz. The crystal size of the support was calculated based on the maximum intense peak of the pattern (2θ=26.75°) and was observed to be 30 nm.

The surface characterization was also carried out by FESEM (Make: Zeiss). Fig. 5 presents the surface FESEM micrographs of the ceramic treated support and SIEP nickel layer deposited with an initial nickel sulfate concentration (C_i) of 0.08 (mol/L). It can be observed that well-developed nickel layers were existent for the membrane. Based on the analysis of the FESEM image using ImageJ software, it was observed that the pores were distributed over wider pore size values and the average pore size of the treated support as evaluated from the ImageJ software was found to be 140 nm which was close to that evaluated from nitrogen permeation (90–120 nm), respectively.

4.2. Feasibility of the ceramic support

Fig. 6 presents the nitrogen flux profiles for various combinations of average membrane pore size and effective

porosity for various cases. As shown, for a nickel dense film thickness of 1 μm, the feasible combinations of porosity ((ε/q^2) min) varied from 4.5×10^{-2} to 1.1×10^{-3} for pore diameter (d_p) variation from 20 nm to 500 nm, respectively. However, when the nickel film thickness was enhanced 5-fold (to 5 μm), (ε/q^2) min varied from 9.1×10^{-3} to 2.2×10^{-4} for d_p variation from 20 nm to 500 nm, for a film thickness of 10 μm, (ε/q^2) min varied from 4.5×0^{-3} to 1.1×10^{-4} for d_p variation from 20 nm to 500 nm and for a film thickness of 20 μm, (ε/q^2) min varied from 2.2×10^{-3} to 5.6×10^{-5} for d_p variation from 20 nm to 500 nm, respectively. The obtained membrane morphological parameters indicated that the raw support was feasible for a desired minimal dense nickel film thickness of 1 μm and the treated support was feasible for a desired minimal dense nickel film thickness of 5 μm. These theoretical deductions indicated that irrespective of the fabrication method, the supports were feasible for very low values of dense metal film thickness on the supports which was very difficult to achieve using conventional and novel metal deposition methods on porous ceramic supports with achieved morphologies.

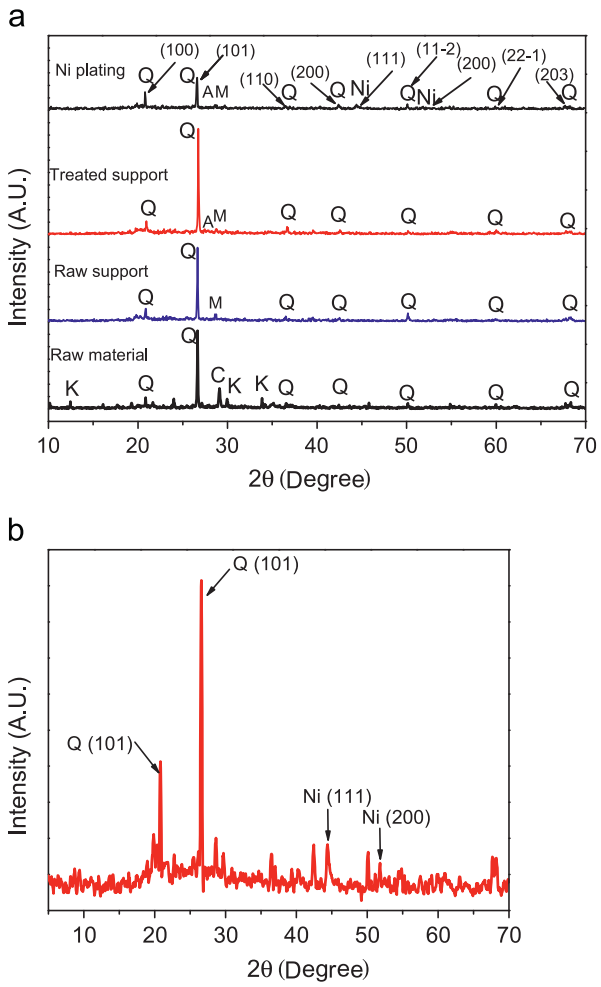

Fig. 4. (a) XRD patterns of raw material mixture, sintered raw support, sintered treated (NaOH) support and the nickel membrane (b) XRD pattern of Nickel membrane.

4.3. Synchronity for nickel plating (average flux and percent pore densification)

Fig. 7(a) represents the average flux data trends with respect to the time of plating. The average flux through the membrane reduced from 4.1×10^{-2} to 2.1×10^{-2} (mol/m^2/s) in 24 h for M_1 (SOEP), 3.0×10^{-2}–1.5×10^{-3} (mol/m^2/s) in 24 h for M_2 (SIEP), 1.8×10^{-1}–3.7×10^{-3} (mol/m^2/s) in 24 h for M_3 (SIEP) and 2.2×10^{-1}–3.6×10^{-2} (mol/m^2/s) in 24 h for M_4 (SOEP), respectively. It was observed that for membranes M_1 and M_2 the initial plating steps increased the average flux through the membrane. This indicated that for these membranes, morphological modifications (opening of voids/pores) were dominant as compared to metal deposition inside the porous structure. Eventually with increment in plating hours it was observed that morphological modifications became minimal and pore densification gradually improved. Further for the treated membrane M_3 (SIEP) it was observed that after 24 h of plating the ratio of initial flux to the final flux was around 48.8 which was quite higher than the value obtained for M_4 membrane (6.2).

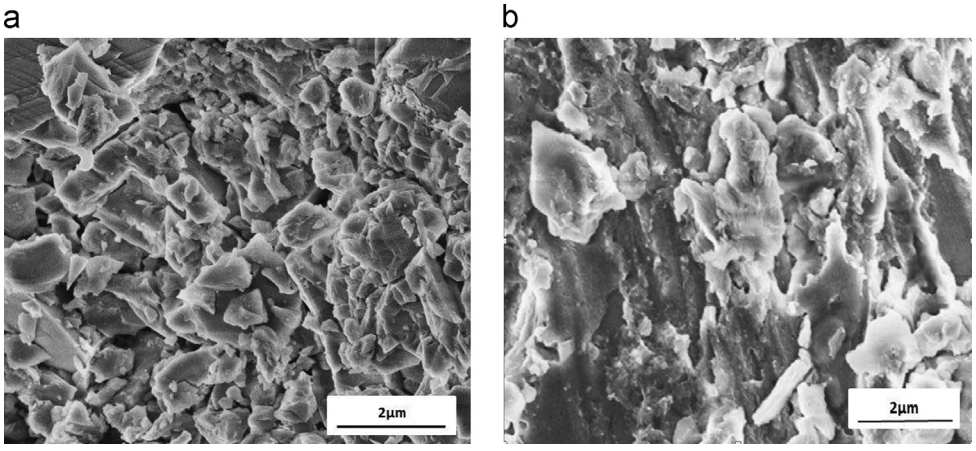

Fig. 5. Surface FESEM micrographs of (a) treated support (b) SIEP membrane (M_3).

The time dependent enhancement and reduction in average membrane flux for membranes M_1 and M_2 clearly depicted that the low cost ceramic supports were not compatible enough to handle the plating process and therefore, the supports required further treatment so that the supports could withstand the corrosive environment that prevailed during the long term exposure of electroless plating in a highly alkaline environment. Various possible reasons for opening of pores correspond to surface and pore modifications of the substrate at the plating conditions. Therefore, the NaOH pretreatment was regarded to be a viable option to make the supports feasible for low cost dense metal ceramic composite membrane research.

Fig. 7(b) presents the time dependency with respect to percent pore densification trends. *PPD* values varied from 0% to 46.7% in 24 h for M_1 (SOEP), 0% to 95% in 24 h for M_2 (SIEP), 0% to 98% in 24 h for M_3 (SIEP) and 0% to 83.9% in 24 h for M_4 (SOEP). Further the *PPD* values for M_1 and M_2 were initially observed to be negative indicating to the fact that the rate of pore opening was faster than the rate of pore densification thereby confirming that membrane healing process was too slow for the raw supports. However, plating in the later hours indicated that positive profiles were observed for M_1 and M_2 which clearly indicated that SOEP and SIEP processes not only repaired the damage morphologies but also densified the membranes. But this was not the case with NaOH treated supports where systematic reduction in flux was observed with plating time. However, excessive deposition of nickel in the ceramic matrix is not desired for the functional supports, as this could lead to higher thermal stresses that could be induced with temperature cycling phenomena for the Pd composite membranes.

Even for the raw supports, for the same time of plating (24 h), SIEP (M_2) reduced the *PPD* twice as compared to SOEP (M_1). Thus it can also be concluded that surfactant played an important role in reducing the average flux through the membrane and served better than sonication in achieving densification both for the raw and the treated supports. Therefore, more detailed research in process engineering of materials manufacturing processes involving surfactants is as well needed.

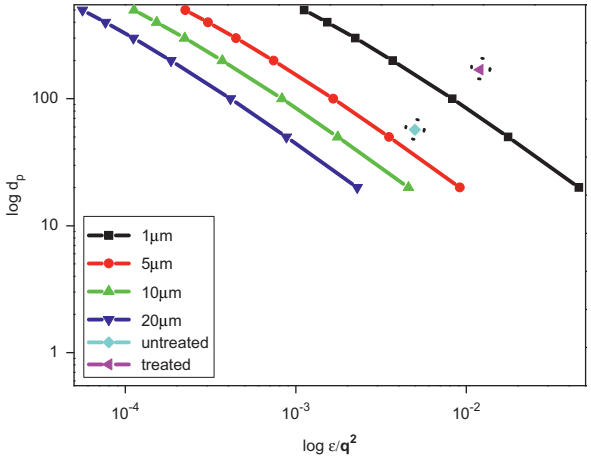

Fig. 6. Log d_p vs. log (ε/q^2).

5. Conclusions

This work presented an integrated experimental and theoretical approach for the development of compatible functional supports towards dense metal ceramic composite membrane fabrication. The challenging scenario of this study was to work with laboratory fabricated supports characterized with lower combinations of average pore size and lower effective porosity. For such supports etching in alkaline medium served to be favourable in terms of compatibility of the support and corrosion resistance. NaOH treatment prior to plating enabled enlargement of the membrane pores to its target diameter such that the early plating steps does not serve as a treatment steps for the supports. Further XRD patterns clearly indicated that NaOH treatment increased the crystalinity of the raw materials thereby enhancing the pore size and porosity of the membrane. Moreover the morphological fitness of the ceramic support clearly indicated that the supports were feasible for very low values of dense metal film thickness irrespective of the fabrication technique. The fabricated nickel composite membranes were anticipated to serve as functional supports for dense palladium membranes. A tentative combination of optimal support morphological properties and optimal electroless plating process as highlighted in this article would be

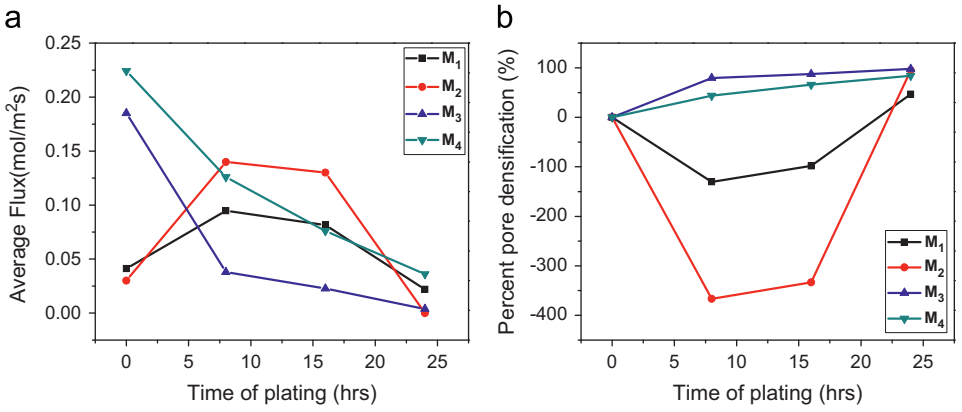

Fig. 7. Performance of nickel plated membranes in terms of time dependent (a) average flux and (b) PPD.

useful to serve as a guideline for the realization of low cost multi-metal composite membranes.

Nomenclature

$Perm_{lit}$	Maximum hydrogen permeability of the nickel film reported in the literature (mol/m^2/s/Pa$^{0.5}$)
δ_{lit}	Critical dense nickel film thickness in the literature (μm)
δ_{ass}	10 μm (μm)
n'	Exponent (=0.5 according to Stewart's law)
A_m	Permeable area of the membrane (m^2)
Q	Volumetric flow rate (m^3/s)
P_2	Membrane pressure at permeate side (Pa)
ΔP	Trans-membrane pressure drop (Pa)
d_p	Average pore size (μm)
(ε/q^2)	Effective porosity
$\overline{P}$	Average pressure on the membrane (Pa)
v	Molecular mean velocity of the gas (m/s)
l	Pore length (m)
q	Tortuosity
η	Viscosity of gas (Pa s)
K	Effective permeability factor (m/s)
J	Flux through the membrane (mol/m^2/s)
$\overline{J}$	Average flux through the membrane (mol/m^2/s)
i	Hour of nickel plating (as exponent)
$\overline{J}_0$	Average flux through the support (mol/m^2/s)
$\overline{J}_i$	Average flux through the membrane after ith hour of nickel plating (mol/m^2/s)
PPD	Percent pore densification (%)
ELP	Electroless plating
SIEP	Surfactant induced electroless plating
SOEP	Sonication induced electroless plating

Acknowledgements

This work is partially supported by a grant from the DST (Department of Science and Technology) New Delhi. Any opinions, findings and conclusions expressed in this paper are those of the authors and do not necessarily reflect the views of DST, New Delhi. Special thanks to Dibjyoti Saloi who worked as project assistant and helped us for this work.

References

[1] M. Kitiwan, D. Atong, Effects of porous alumina support and plating time on electroless plating of palladium membrane, Journal of Materials Science & Technology 26 (2010) 1148–1152.
[2] L.L.O. Silva, D.C.L. Vasconcelos, E.H.M. Nunes, L. Caldeira, V. C. Costa, A.P. Musse, S.A. Hatimondi, J.F. Nascimento, W. Grava, W. L. Vasconcelos, Processing, structural characterization and performance of alumina supports used in ceramic membranes, Ceramics International 38 (2012) 1943–1949.
[3] N. Kishore, S. Sachan, K.N. Rai, A. Kumar, Synthesis and characterization of a nanofiltration carbon membrane derived from phenol-formaldehyde resin, Carbon 41 (2003) 2961–2972.
[4] G.T.P. Mabande, G. Pradhan, C. Schwieger, M. Hanebuth, R. Dittmeyer, T. Selvam, A. Zampieri, H. Baser, R. Herrmann, A study of silicalite-1 and Al-ZSM-5 membrane synthesis on stainless steel supports, Microporous and Mesoporous Materials 75 (2004) 209.
[5] A. Potdar, A. Shukla, A. Kumar, Effect of gas phase modification of analcime zeolite composite membrane on separation of surfactant by ultrafiltration, Journal of Membrane Science 210 (2002) 209–225.
[6] S. Jha, K.L. Rubow, Nickel microfiltration media for gas and liquid filtration, Advances in Filtration and Separation Technology 13 (1999) 512–520.
[7] S.K. Ryi, J.S. Park, S.J. Park, D.G. Lee, S.H. Kim, Fabrication of nickel filter made by uniaxial pressing process for gas purification: fabrication pressure effect, Journal of Membrane Science 299 (2007) 174–180.
[8] D. Vasanth, G. Pugazenthi, R. Uppaluri, Fabrication and properties of low cost ceramic microfiltration membranes for separation of oil and bacteria from its solution, Journal of Membrane Science 379 (2011) 154–163.
[9] Wen-Hsiung Lin, Ying-Chi Liu, Hsin-Fu Chang, Autothermal reforming of ethanol in a Pd–Ag/Ni composite membrane reactor, International Journal of Hydrogen Energy 35 (2010) 12961–12962.
[10] B. Ernst, S. Haag, M. Burgard, Permselectivity of a nickel/ceramic composite membrane at elevated temperatures: a new prospect in hydrogen separation?, Journal of Membrane Science 288 (2007) 208–217
[11] V.K. Bulasara., M.S. Abhimanyu, T. Pranav, R. Uppaluri, M.K. Purkait, Performance characteristics of hydrothermal and sonication assisted electroless plating baths for nickel–ceramic composite membrane fabrication, Desalination 284 (2012) 77–85.
[12] V.K. Bulasara, R. Uppaluri, H. Thakuria, M.K. Purkait, Nickel–ceramic composite membranes: optimization of hydrazine based electroless plating process parameters, Desalination 275 (2011) 243–251.
[13] Altunoglu, Abdulkadir, Hydrogen Permeation Through Nickel and Nickel Alloys: Surface Reactions and Trapping, Ph.D. Thesis, The Open University, (1994).
[14] K.S.W. Sing, D.H. Everett, R.A.W. Haul, L. Moscou, R.A. Pierotti, J. Rouquerol, T. Siemieniewska, Reporting physisorption data for gas/solid systems with special reference to the determination of surface area and porosity, Pure and Applied Chemistry 57 (1985) 603–619.
[15] M.L. Granizo, M.T.B. Varela, S. Martinez-Ramirez, Alkali activation of metakaolins: parameters affecting mechanical, structural and microstructural properties, Journal of Materials Science 42 (2007) 2934–2945.
[16] J.G.S. van Jaarsveld, J.S.J. van Deventer, G.C. Lukey, The effect of composition and temperature on the properties of fly-ash and kaolinite-based geopolymers, Chemical Engineering Journal 89 (2002) 63–73.